Materials Today Bio 20 (2023) 100665

Contents lists available at ScienceDirect

Materials Today Bio

journal homepage: www.journals.elsevier.com/materials-today-bio

Ultrasonic/electrical dual stimulation response nanocomposite bioelectret for controlled precision drug release

Junfei Li [a], Yajie Xie [a], Xiaoran Zou [a], Zhengze Li [a], Wenbo Liu [a,b], Guodong Liu [a], Mengjiao Ma [a], Yudong Zheng [a,*]

[a] School of Materials Science and Engineering, University of Science and Technology Beijing, Beijing, 100083, China
[b] Center for Medical Device Evaluation, National Medical Products Administration, Intellectual Property Publishing House Mansion, Qixiang Road, Haidian District, Beijing, China

ARTICLE INFO

Keywords:
Flexible bioelectret
Charge density
Double stimulation response
Drug release

ABSTRACT

Electret materials have attracted extensive attention because of their permanent polarization and electrostatic effect. However, it is one of problem that needs to be solved in biological application to manipulate the change of surface charge of electret by external stimulation. In this work, a drug-loaded electret with flexibility and no cytotoxicity was prepared under relatively mild conditions. The electret can release the charge through stress change and ultrasonic stimulation, and the drug release can be accurately controlled with the help of ultrasonic and electric double stimulation response. Here, the dipoles like particles of carnauba wax nanoparticles (nCW) are fixed in the matrix based on the interpenetrating polymer network structure, and "frozen" oriented dipolar particles that are treated by thermal polarization and cooled at high field strength. Subsequently, the charge density of the prepared composite electret can reach 101.1 nC/m^2 at the initial stage of polarization and 21.1 nC/m^2 after 3 weeks. In addition, the stimulated change of electret surface charge flow under cyclic tensile stress and cyclic compressive stress can generate a current of 0.187 nA and 0.105 nA at most. The ultrasonic stimulation results show that when the ultrasonic emission power was 90% (P_{max} = 1200 W), the current of 0.472 nA can be generated. Finally, the drug release characteristics and biocompatibility of the nCW composite electret containing curcumin were tested. The results showed that it not only had the ability to accurately control the release by ultrasound, but also triggered the electrical effect of the material. The prepared drug loaded composite bioelectret provides a new way for the construction, design and testing of the bioelectret. Its ultrasonic and electrical double stimulation response can be accurately controlled and released as required, and it has broad application prospects.

1. Introduction

In 1732, Gray predicated that there might be a kind of "permanent attraction" material in the dielectric [1]. In 1892, similar to magnetic materials, Oliver Heaviside referred to dielectric materials capable of exhibiting permanent polarization as "electrets" [2]. Since the artificial electret (carnauba wax electret) was first manufactured by thermal polarization method in 1919 [3], electrets have been applied to the fields of dielectric physics, sensor engineering and biomedicine [4–11]. At present, the research of electret materials, the development of devices and their application in various fields have entered a period of diversification of organic materials, inorganic materials, composite materials and biomaterials [12–14].

Similar to many functional materials, in many cases, biomaterials are subjected to an electrode treatment to obtain a bioelectret. The biological effects produced by electrets (piezoelectric, pyroelectric and ferroelectric effects) have been widely used in the fields as tissue repair [8], biosensors [5,15] and intelligent biomedical equipment [16]. Here, the electret, as an external electrical stimulation, mainly uses piezoelectric effect, electrostatic effect and local micro-current to play its role. The electrostatic field of electret mainly comes from the electric field generated by the external space charge of the material and the electric field generated by the internal dipole charge inside the material [17]. The piezoelectric effect of electret is mainly due to the change of induced charge density at both ends of the material due to the strain when the material is subjected to tensile stress and compressive stress, which leads to the change of electric field [18]. Since 1950s, many studies have introduced bioelectret as external electrical stimulation, which can compensate or regulate the

* Corresponding author.
E-mail address: zhengyudong@mater.ustb.edu.cn (Y. Zheng).

https://doi.org/10.1016/j.mtbio.2023.100665
Received 11 February 2023; Received in revised form 8 May 2023; Accepted 12 May 2023
Available online 13 May 2023

electret state of human microenvironment by spontaneously generating micro-electric fields and micro-currents, thus improving blood microcirculation, anti-thrombosis, improving blood vessel wall permeability, promoting bone growth and fracture healing [19,20], promoting percutaneous absorption of drugs [21], and controlling drug release in vitro [22], and so on.

Polymer electret materials have the advantages of flexibility, low density, low cost, and easy structure regulation, which have been paid extensive attention in recent years [23], especially the design, development and research of bio-based electret. Bio-based electret, such as chitosan [24], hyaluronic acid [25], polylactic acid [26], hydroxyapatite [27,28], natural cellulose and so on, have attracted much attention because of their better biocompatibility. However, bio-based electret polarization has some defects, such as low charge density, short life and fast discharge, which often cannot meet its application requirements.

Doping nano-fillers into polymer matrix can improve the charge storage trap [29]. The method is effective and easy to operate, and has great research value and application prospects in improving the charge density of electret storage. The addition of nanoparticles will lead to more hole charge traps at the junction of crystalline and amorphous regions [30–32]. Secondly, there will be chain entanglement and chain curl between nano-particles and polymer molecular chains, which will produce physical defects at the interface and form a large number of interface cavity traps [33]. In addition, chemical bonds on the surface of nano-fillers can also produce traps, including covalent bonds, ionic bonds, coordination bonds, hydrogen bonds, electrostatic interactions, hydrophobic and hydrophilic balances and Van der Waals forces. The doping of nano-fillers can provide more charge traps, thus improving the charge density. However, nano-fillers, such as barium titanate, calcium copper titanate, titanium dioxide, carbon nanotubes, graphene, boron nitride and so on, are widely used [34,35]. However, the biological safety of inorganic nano-materials represented by carbon, metal, ceramics and semiconductor in clinical application has become a big problem. Most of these materials will show acute and chronic cytotoxicity. For example, the integrity of cell membrane and organelle is destroyed, the genetic toxicity of cell nucleus and the production of reactive oxygen species (ROS) in cells [36].

Carnauba wax (CW) is a classical electret material, but its application is limited due to its inherent irresistible shortcomings (such as low working temperature, large volume, etc.). In this paper, we reported a drug loaded composite polymer electret that uses carnauba wax nanoparticles (nCW) as a dipole, which is flexible and non-toxic, and can stimulate change of electret surface charge through stress changes and ultrasound, and can accurately regulate drug release by ultrasonic electrical double stimulation response. Firstly, the nCW was prepared by emulsion phase separation method, and it was "locked" in the interpenetrating network structure matrix composed of polyvinyl alcohol (PVA) and polyacrylamide (PAAm). Then, the nCW dipole like in the "frozen" orientation matrix were by the thermal polarization method to prepare a composite bioelectret. The nanoparticle effect in the composite increases the charge trap density, thus increasing the charge storage density. The nano-scale polymer network structure "locks" the dipole and improves the charge stability. Continuous and stable electrical signals can be generated under different cyclic stress driving stimuli and ultrasonic (US) driving stimuli with different power. Finally, the drug release characteristics of the composite electret containing nCW/Curcumin (nCW/Cur) were studied. The results showed that the drug release could be controlled accurately under the action of ultrasonic and electric double stimulation. The prepared drug loaded composite electret provides a new way for the construction and application of the electret, and it is expected to achieve accurate drug delivery/release on demand due to its ultrasonic electric double stimulation response.

2. Experimental

2.1. Materials

Acrylamide (AAm, AR), N, N′-methylenebisacrylamide (MBAA), tetramethyl-ethylenediamine (TEMED) and ammonium persulfate (APS) in this sequence. Polyvinyl alcohol powder (PVA, polymerization degree of 1750, hydrolysis >99%) were purchased from Sinopharm Group Co., Ltd (China). Carnauba wax (food grade, flake) was provided Shanghai yiba Chemical Raw Materials Co., LTD. Cell Counting Kit-8 (CCK-8), LG-DMEM and Calcein AM·PI were purchased from Dojindo (Japan), Shanghai yuanye biotechnology Co., Ltd and Shanghai yaji biotechnology Co., Ltd, respectively. Deionized water was offered by University of Science and Technology Beijing. All other reagents were analytical grade and used as received. Curcumin; Span-80.

2.2. Reparation of carnauba wax nanospheres

Solid lipid particles were obtained by slight modification according to the method of Gonzalez Mira [37]. Firstly, an aqueous solution containing 2 wt% emulsifier Span-80 was configured as the continuous phase (water phase). The carnauba wax (1.0000 g) and a certain amount of curcumin heated gently at 85 °C until completely melted, which acted as a dispersed phase (oil phase). Subsequently, the system was added to the water phase (50 mL) under high-speed mechanical stirring and emulsified for 30 min at 85 °C, and rapidly cooled to below normal temperature under stirring conditions, carnauba wax loaded with curcumin gradually solidified into microparticles. Curcumin free solid lipid microparticles were prepared according to the same method and materials. Finally, a series of nanospheres loaded and unloaded with curcumin with different particle sizes were obtained by standing, precipitation, washing and freeze-drying. Table S1 shows that encapsulation and loading rates of curcumin-loaded carnauba wax nanospheres (nCW/Cur).

The encapsulation efficiency and drug loading rate of microspheres were tested by ultraviolet spectrophotometer ultraviolet (UV) spectroscopy (Agilent HP 8453, United States), and then the standard curve of curcumin in water-alcohol solution (v/v = 50:50) at the absorbance of 431.5 nm was obtained (Fig. S4). The equation of the standard curve was $y = 0.06394x + 0.01685$, ($R^2 = 0.999$).

The prepared sample was divided into three parts: In a vacuum filter, the particles were washed three time with ethanol, and the unencapsulated curcumin on the surface of the particles was removed with ethanol, then drying at 60 °C for 6 h. The sample was dissolved in 10 mL methylene chloride and sealed. Meanwhile the encapsulated curcumin was extracted by stirring at room temperature for 24 h. Then, the sample is filtered and dissolved in a certain volume (V) of water and ethanol solution (volume ratio 50:50) through Amicon ultrafiltration filters (Millipore, 100 kDa). The concentration of encapsulated curcumin (C_1) was determined by ultraviolet spectroscopy (Agilent HP 8453, United States) at 431.5 nm. The same process was performed for the unwashed particles to determine the total amount of curcumin (both encapsulated and unencapsulated, C_2). The encapsulation efficiency (EE%) and Loading rate (LR) is determined by equations (1) and (2), respectively:

$$EE\% = \frac{C_1 \cdot V}{C_2 \cdot V} \times 100\% \quad (1)$$

$$LR\% = EE \times \frac{m}{M} \times 100\% \quad (2)$$

where m is the amount of curcumin added to the preparation; M is the amount of solid lipid matrix carnauba wax added, EE is the encapsulation efficiency calculated by formula (1).

2.3. Preparation of DN-gel and DN-gel@nCW composites

The preparation method of PVA/PAAm interpenetrating double gel (DN-gel) is similar to that reported in literature [38], and has been improved based on this method. Firstly, 10 g polyvinyl alcohol was dissolved in 90 mL deionized water and stirred at 90 °C for 3 h to completely dissolve PVA to obtain 10 wt% PVA aqueous solution. After the PVA solution was cooled to room temperature, AAM was added and completely dissolved to obtain homogeneous solutions with mass ratios of PVA and AAm of 1: 8, 3: 8, 5: 8, and 8: 8, respectively. Then ammonium persulfate (APS, 0.007 times), N, N′-methylenebisacrylamide (MBAA, 0.01 times) and tetramethyl-ethylenediamine (TEMED, 0.007 times) were added as initiator, crosslinker and catalyst of AAm respectively in the sequence. Pour the mixed solution into the polytetrafluoroethylene mold for static forming to obtain the pre gel, and put it into the −80 °C refrigerator for quick freezing treatment, and finally freeze-drying for 24 h to form and remove water. The above PVA solution and nCW were stirred evenly, and the DN-gel and nCW of composite material (DN-gel@nCW) was obtained according to the above method in other steps. The composite double network gel with different proportions were prepared and named DN-gel-1, DN-gel-2, DN-gel-3, DN-gel-4, and DN-gel-3@nCW respectively. Table S3 shows that formulations containing different additive levels. The schematic diagram of synthesis is shown in Fig. 1a.

2.4. Breakdown test and thermal poling

The high temperature piezoelectric polarization device (HYJH-G1200-20 kV) is provided by Shaanxi Huiyan New Material Technology Co., LTD. The temperature is maintained by a heat plate, and the poling electric field is applied using a Dc high voltage power supply. Poling electrodes are copper films with 3.0 cm × 3.0 cm × 0.5 cm. The principle diagram of the polarization device is shown in Fig. 1b.

2.5. Characterization and measurement

2.5.1. The fourier transform infrared (FTIR) spectrum

The sample was put into an infrared spectrometer (a TENSOR II spectrometer, Bruker, Germany) for measurement. The spectra were recorded with 32 scans and were calculated in the wavenumber ranging from 4000 to 600 cm^{-1}.

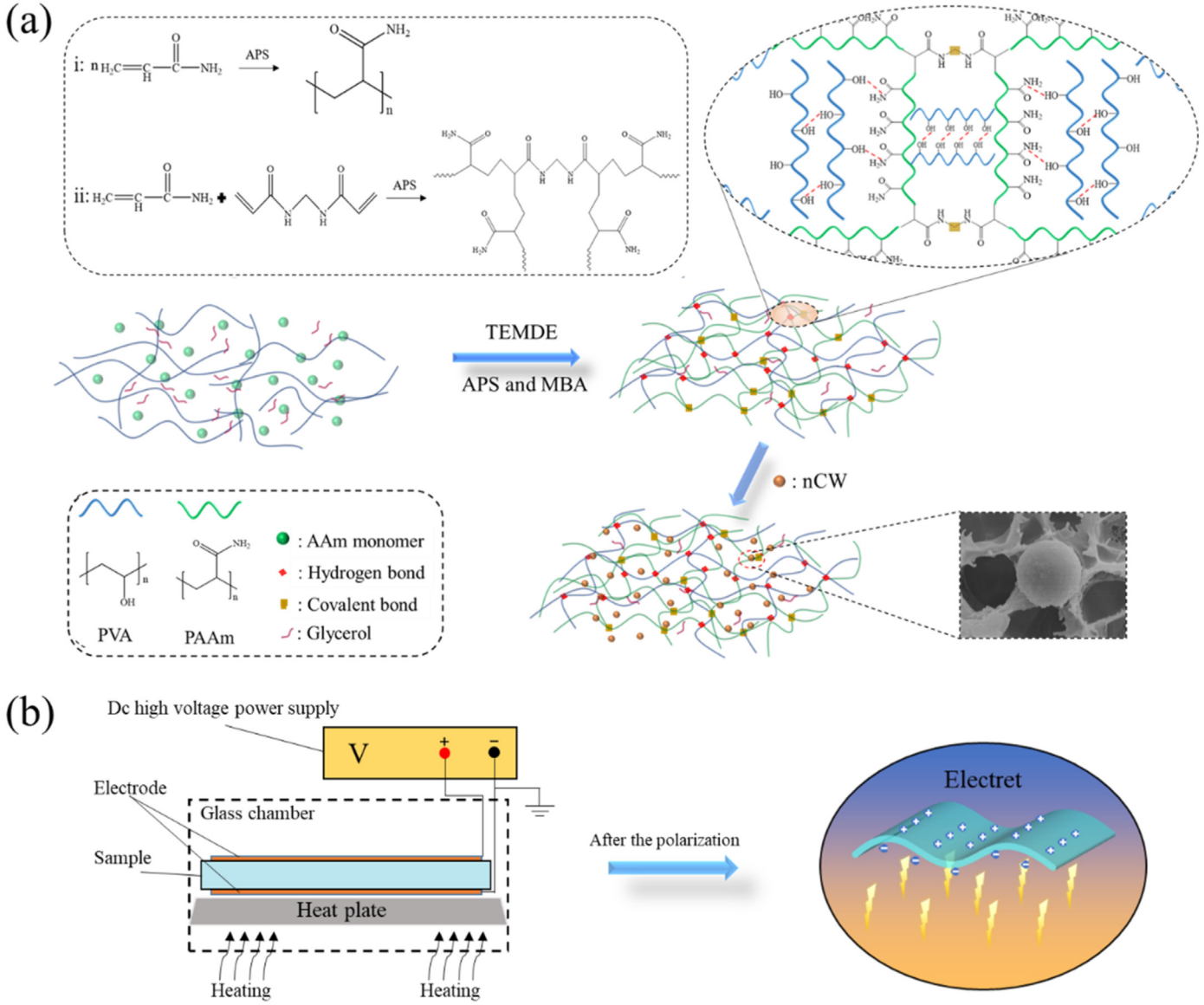

Fig. 1. Preparation of DN-gel@nCW flexible bioelectret. (a) The synthetic scheme of DN-gel@nCW composites. (b) Polarization of DN-gel@nCW flexible bioelectret.

2.5.2. *X-ray diffraction (XRD)*

Crystalline state of the different samples was carried out with an X-ray diffractometer (Rigaku, RAD-3C). We used Cu Kα radiation (Kα = 1.54059 Å) operating at 40 kV and 40 mA. Scanning rate was 4°/min in the scope of 10–50°.

2.5.3. *Scanning electron microscopy (SEM)*

The surface elemental analysis of composites was studied by an energy-dispersive X-ray spectrometer (EDS, Ns-7 Thermo Fisher Scientific, USA) equipped with AURIGA Cross Beam FIB/SEM field emission electron microscopy. And, SEM was also used to analyze microscopic morphology of the samples was observed.

2.5.4. *Differential scanning calorimetry (DSC)*

The melting and crystallization processes of nCW, nCW/Cur, Cur, and physical mixture (CW and Cur) were observed by differential scanning calorimeter. The measurement condition are as follows: firstly, the temperature is raised from 25 °C to 400 °C, the melting process of the sample is observed, the temperature is kept for 5 min, and then the temperature is lowered to 25 °C, and the crystallization process of the sample is observed. The protective atmosphere is nitrogen, the mass of the sample is about 10 mg, and the heating speed is 10 °C/min.

2.5.5. *Mechanical property*

Tensile tests were measured on a CMT4204 microcomputer control electronic universal testing machine (Shenzhen century tianyuan instrument Co. LTD, China) according to GB/T 16,491–2008 at a crosshead speed of 10 mm min^{-1}. Test at least three samples per sample and report average results.

2.5.6. *Electrical measurement*

The charge was measured by a charge amplifier (Kistler 5018A, Germany), whose amplification ratio is set to be 500 pC V^{-1}. An oscilloscope (KEYSIGHT DSO1004A, America) is connected in series to detect the charge flow.

2.5.7. *Dielectric performance measurements*

A broad frequency dielectric spectrometer Agilent4294A (Novocontrol, the United States) was used to measure the dielectric properties of the composites. The measurements were carried out at room temperature, a frequency range of 40–10^7 Hz and an operating voltage of 220 V. The circular sample was cut from the compression molded slice and it had a diameter of 10 mm and a thickness of 0.7 mm. Before measurement, the top and lower surfaces of sample were coated by gold, which acted as the electrodes during the measurements.

2.5.8. *Output charge signal measurement by mechanical and ultrasonic stimuli*

To measure output charge signal by mechanical stimuli, we use carbon conductive adhesive as a stretchable electrode, which is plated on the bottom of the flexible electret and sealed in Ecoflex (0030) insulating silica gel. Then, connect the electrode end of the encapsulated sample with one end of the charge amplifier (Kistler 5018A), and the other end is grounded. Connect the output of the charge amplifier to an oscilloscope (KEYSIGHT DSO1004A). Set different cyclic stretching or cyclic compression rates with mechanical instruments, and observe the change of electric charge.

Similarly, copper electrodes are plated on the bottom of the flexible electret and sealed in Ecoflex insulating silica gel. The output charge signal of the flexible bioelectret were measured by a charge amplifier. The intensity of ultrasound waves was measured using an ultrasonic power meter (Ultrasonic Equipment, JY98-IIIN, China) in water. The ultrasound waves were generated by tip-sonicator (Ningbo Scientz Biotechnology co., LTD, diameter of the tip is 15 mm) with a power amplitude of 10%, 30%, 50%, and 90% (P_{max} = 1200 W), respectively.

2.5.9. *Biocompatibility*

Using cell culture method to evaluate the cytotoxicity and cell adhesion of medical biomaterials is a widely used method, which has the advantages of simplicity, rapidness and resource saving. The chemically enhanced double cross-linked hydrogel material was co-cultured with mouse fibroblasts (L929), and the cellular compatibility of the material was studied by CCK-8 method, observation of cell growth morphology and fluorescent staining.

3. Results and discussion

3.1. *Preparation and characterization of carnauba wax nanoparticles*

Table S1 and Fig. 2 shows the influence of different stirring speeds on the particle size distribution, polydispersity index and Zeta potential of carnauba wax microcapsules. It can be seen that the average particle size of nanospheres decreases with the increase of stirring speed, and the average particle size of nCW-1, nCW-2, nCW-3 and nCW-4 are 420 ± 15 nm, 361 ± 8 nm, 299 ± 11 nm and 272 ± 7 nm, respectively. According to the grain size distribution diagrams of Fig. 2b and c, the grain size distribution range of nCW-1 and nCW-2 is wide, while that of nCW-3 (see Fig. 2d) and nCW-4 (see Fig. 2e) is narrow and relatively uniform. This is mainly that due to the low cohesive energy of carnauba wax to form stable and uniform wax drops under the action of high-speed mechanical shearing force. However, at 1000 rpm, the average particle size of nCW-5 emulsified for 60 min is slightly smaller than that of nCW-4, and the particle size distribution range is wider (see Fig. 2f). This is because long-term emulsification increasing the collision between particles, resulting in particle agglomeration. The zeta potential of carnauba wax nanospheres was approximately around −40 mV, and the emulsion stability was enhanced when the rotation speed increased. The absolute value of zeta potential increased, and the inter particle electrostatic repulsion increased.

3.2. *Characterization for DN-gel and DN-gel@nCW composites*

The manufacturing process of DN-gel with double interpenetrating network structure is shown in Fig. 1a. AAm monomers were polymerized by free radical polymerization, forming a chemically crosslinked first-order PAAm polymer crosslinked network structures. Meanwhile, based on the hydrogen bonding interactions between the amide groups in the PAAm polymer chains and the hydroxyl groups of PVA and glycerol molecules, a second physical cross-linked network structure interpenetrating with the PAAm polymer network structure was formed inside the gel, thus constructing a gel with a double network interpenetrating structure. Among them, chemically crosslinked PAAm network structure endows the composite gel with excellent mechanical properties, while its dynamic and reversible physical crosslinked network structure endows the composite gel with excellent elasticity and recovery ability.

Cold field emission scanning electron microscopy is used to provide the morphological and structural characteristics of hydrogel electrolytes. Fig. 3a show the macro and micro morphology and EDS spectra of different gel complexes. With the increase of PVA content, the transparency of the composite gel decreases, which may be the result from the formation of microcrystalline structure of PVA network in the composite gel. Observation of the composite gels using cold field scanning electron microscopy showed that all hydrogels exhibited typical three-dimensional honeycomb-like structures. Among them, DN-gel-1 has the largest and uneven average pore diameter; Compared with DN-gel-1, with the increase of PVA content, the micropores of DN-gel-2, DN-gel-3 and DN-gel-4 composite gels are more uniform and compact. This mechanism is also considered to reduce the distance between PVA chains and promote the formation of hydrogen bonds and crystallization. This change of network structure can effectively maintain the stability of the sample and reduce the slip between chain segments [39]. In addition, by scanning the energy spectrum of elements, it can be observed that C, N,

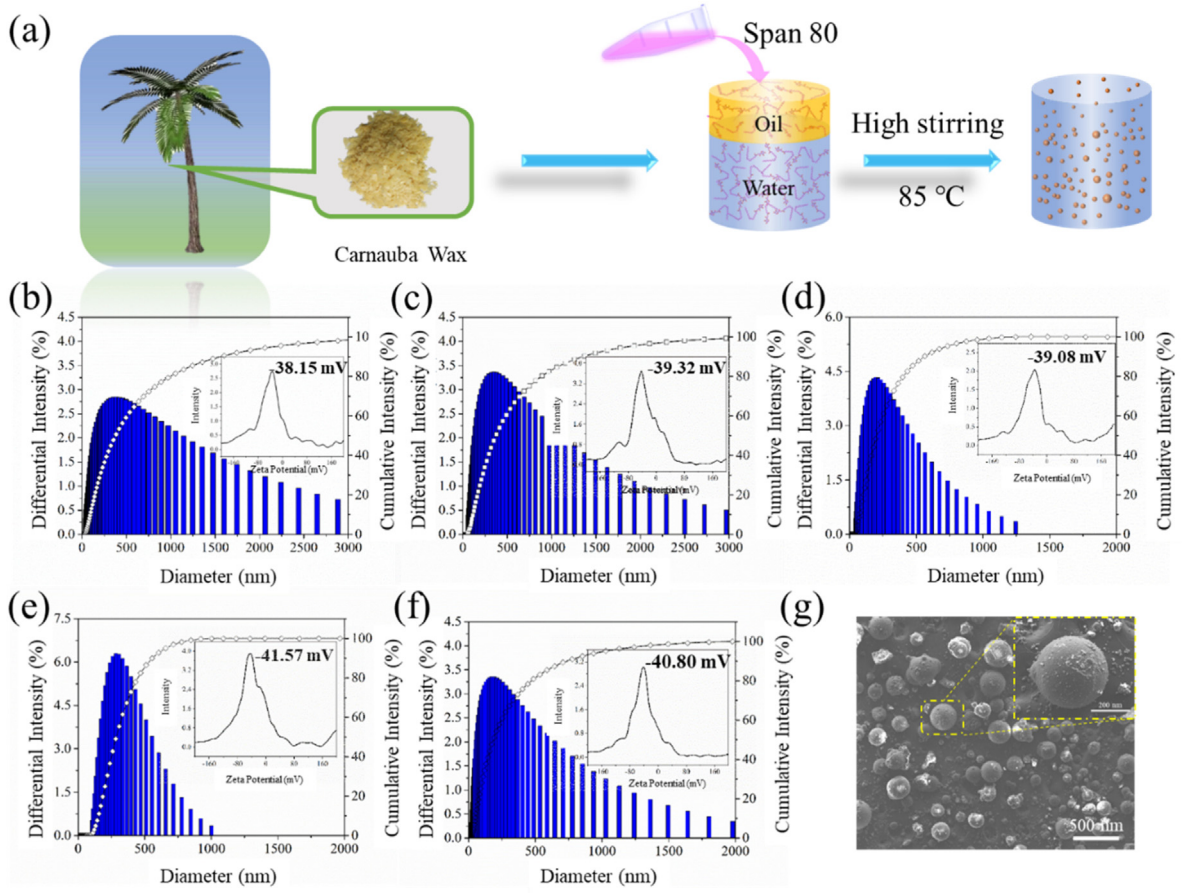

Fig. 2. (a) Preparation of carnauba wax microcapsule. The particle size and zeta potential of (b) nCW-1, (c) nCW-2, (d) nCW-3, (e) nCW-4, and (f) nCW-5 respectively. (g) The SEM microscopic image of the morphology of nCW.

and O elements are uniformly dispersed on the surface of DN-gel-3 sample, which also indicates that the PVA network and PAAM network are well entangled and crosslinked, and their cross-network structure is stable.

The infrared spectra of DN-gel composites are shown in Fig. 3b. In DN-gel composites, N–H asymmetric stretching peak is found at 3395 cm^{-1}, and the symmetric stretching peak for N–H is at 3197 cm^{-1}. The stretching vibration peak of C═O in the amide bond is at 1672 cm^{-1}, while the absorption peak at 1613 cm^{-1} is caused by the deformation vibration of N–H [40]. The peak of 846 cm^{-1} is the characteristic peak of PVA isotactic sequence, the intensity of this peak weakened in PVA/-PAAM composite gel, indicating that PVA was in a disordered state in DN-gel composites, entangled with PAAM network and partially copolymerized. The peak of 1096 cm^{-1} is the absorption peak of C–O single bond contraction and O–H bending vibration [41]. The strength weakening of this peak in DN-gel composites, which is due to the free radical graft copolymerization of PVA and PAAm monomers. This result shows that PVA and PAAM are not simply mixed, but form hydrogen bond stable entanglement in their respective molecular networks.

Different amount of PVA and PAAM double network gel have very similar diffraction patterns. It can be seen from Fig. 3c that the sample has a large diffraction peak at $2\theta = 19.4°$ and a shoulder peak at $2\theta = 22.6°$, corresponding to (101) and (200) planes of PVA crystal respectively. The absorption peak appears at $2\theta = 41°$, indicating the internal hydrogen bond reconstruction of the sample [42]. In DN-gel sample, with the increase of PVA content, the intensity of diffraction peaks at (101) and (200) planes gradually increased, indicating that acrylamide monomer had no effect on the crystallinity of PVA in the process of forming polymer network.

In addition, the swelling properties of DN-gel with different PVA contents were measured (Fig. 3d). DN-gel composite crosslinking network reached water retention state after soaking for about 24h, and reached swelling equilibrium after soaking for 72h. As expected, DN-gel with high PVA content showed a lower equilibrium swelling rate, indicating an increase in network density. This result is consistent with the microstructure of DN-gel under electron microscope. Meanwhile, the test results of contact angles of different composite gels are shown in Fig. 3e. The results showed that the contact Angle decreased and the hydrophilicity increased with the increase of PVA content.

Based on the above analysis of the properties of the composite gel, it can be seen that the interpenetrating network structure of DN-gel-3 and DN-gel-4 gels was stable. In addition, Fig. S1 shows the 3D network pore size distribution of the composite gel. It can be seen that the average Cross-linking network pore size of DN-gel-3 was 1.01 μm, and most of the pore size are distributed in the range of 0.5–1.5 μm. In order to stabilize the CW nanospheres in the gel network structure, combined with the particle size of nCW microspheres, the obtained nCW-4 and DN-gel-3 were compounded to obtain DN-gel-3@nCW composite gel. Subsequently, the structure and characteristics of DN-gel-3@nCW were characterized. As shown in Fig. S2, effects of different amounts of nCW added on the mechanical and hydrophilic properties of composite matrix. Based on this, we chose to add 0.2 g of nCW particles to the matrix DN-gel-3 (i.e., DN-gel-3@nCW sample). Fig. 3a show that DN-gel-3@nCW the physical and SEM images of the composite gel can be seen to be translucent, and the carnauba wax nanospheres are uniformly dispersed in the gel network structure. As shown in Fig. 3c, DN-gel-3@nCW the composite gel has new characteristic peaks at 21.5° and 23.8°, which are characteristic peaks of carnauba wax nanospheres by X-ray diffraction

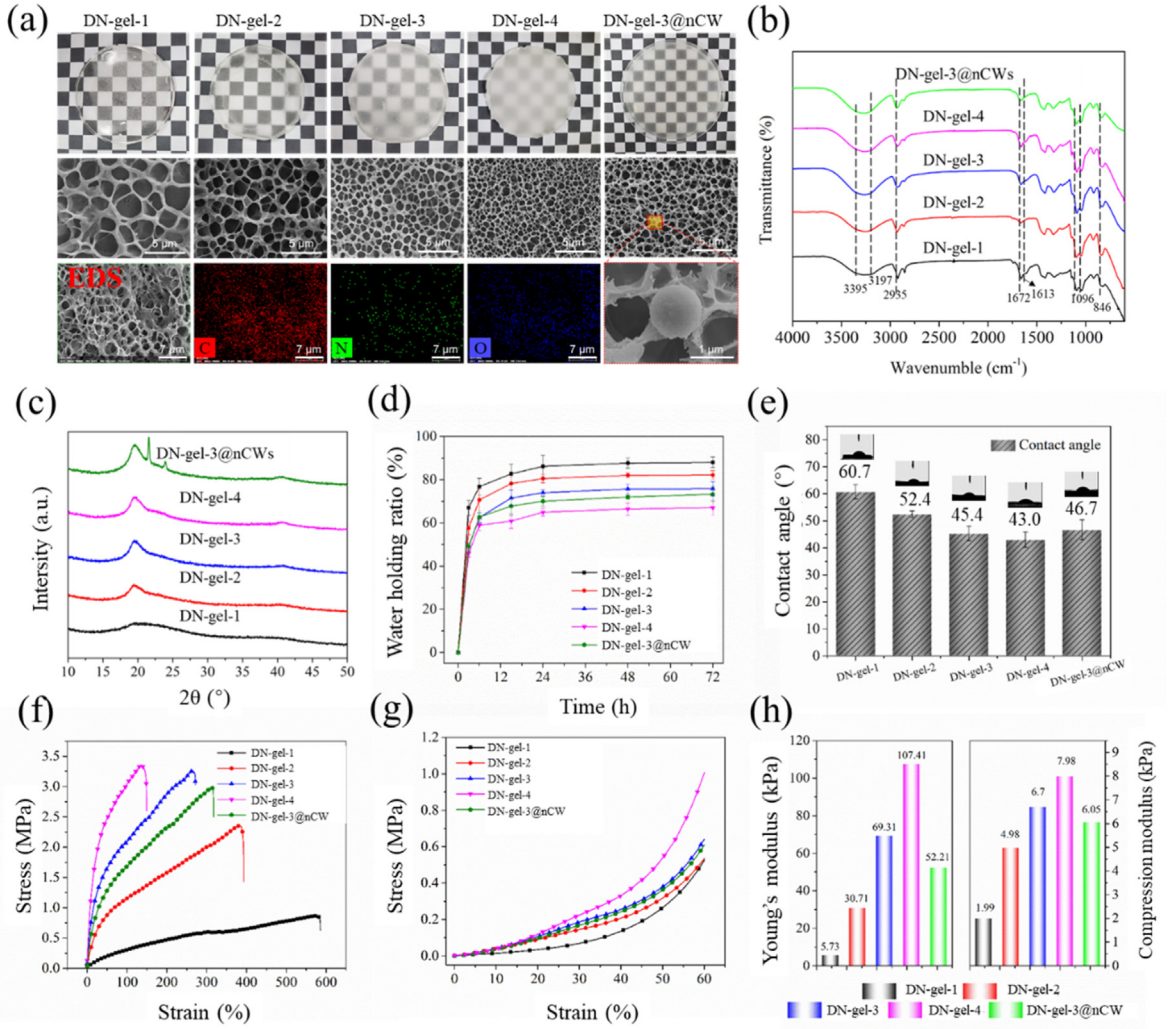

Fig. 3. Characterization for DN-gel composites. (a) Macroscopic, microscopic SEM images and EDS, (b) FTIR, (c) XRD, (d) The water holding ratio, (e) Contact angle (f) Tensile stress-strain curve and (g) Compression stress-strain curve, (h) Young's modulus and Compression modulus of DN-gel-1, DN-gel-2, DN-gel-3, DN-gel-4, and DN-gel-3@nCW composite.

[43]. In addition, compared with DN-gel-3, it also reduced the swelling ratio and water absorption of the gel after adding carnauba wax nanospheres (see Fig. 3d) at the same time, the contact angle increases and hydrophilicity decreased.

Mechanical properties of DN-gel composites: Tensile and compressive properties of different the DN-gel sample and its composites were tested, and the obtained tensile stress-strain curves and compressive stress-strain curves are shown in Fig. 3f and g. Fig. 3h shows the key parameters of the tensile and compression curves and Young's modulus and compression modulus. With the increase of PVA content, the mechanical tensile strength increases gradually, but the elongation at break decreases, and the Young's modulus increases gradually. It shows that PVA makes the composite double network gel gradually change from “soft and tough” to “hard and brittle”, so the mechanical properties of gel can be adjusted by adjusting different proportions. Although the tensile strength of DN-gel-4 was increased by 285.3% compared with that of DN-gel-1 sample, the elongation at break decreased by 76.4%. The tensile strength of DN-gel-3 increased by 204.9%, and the elongation at break decreased by 54.3% compared with DN-gel-1, but the Young's modulus increased by 1115.8%. The results showed that the increase of the density of PVA PAAM interpenetrating network made the gel hard and brittle. In addition, the compression performance test results show that the compression strengths of DN-gel-1, DN-gel-2, DN-gel-3 and DN-gel-4 under 60% strain are respectively 526.1 kPa, 535.9 kPa, 641.3 kPa and 1005.2 kPa (increased by 91.1%), showing a similar law to the tensile strength. This is due to the increase of crosslinking density caused by the increase of PVA content [38].

On the basis of the mass ratio of PVA to AAm DN-gel-3@nCW composite gel of 5: 8, the nCW composite was obtained in cross-linked network. The results showed that the tensile strength and elongation at break increase from 2657.1 kPa to 262.0% to 2935.2 kPa and 282.8%, respectively, while the Young's modulus decreases from 69.3 kPa to 52.2 kPa. This situation is mainly due to the gel network structure under the mass ratio of PVA to AAM of 5: 8, which has a good combination effect on carnauba wax nanospheres. When the carnauba wax nanospheres are broken under tension, they will hinder the cracks propagation, thus improving the tensile strength and elongation at break. The decrease of Young's modulus is mainly due to the stress concentration of particles in the matrix during the stretching process, and a large amount of deformation work is absorbed during the yield process, thus resulting in toughening [44]. Compared with DN-gel-3 samples, the compressive strength and elastic modulus of composite carnauba wax nanospheres under 60% strain decreased by 5.1% and 9.0%, respectively. This is because in the process of compression, the compressive strength of carnauba wax nanospheres is lower than that of the matrix, and the nanospheres occupy a certain proportion in the matrix, thus reducing the

compressibility of the material. It can be seen that the composite of carnauba wax nanospheres has a positive effect on the tensile mechanical properties of the matrix material and a negative effect on the compressive mechanical properties, but it is only slightly lower than before.

3.3. Polarization characteristics of the polarized DN-gel composites

Materials in the environment of electric field will have the possibility of breakdown, so it is very necessary to understand the breakdown mechanism of materials. When the electric field intensity applied by the dielectric reaches a critical value, the dielectric will change from dielectric state to conductive state, which is called dielectric breakdown. Fig. 4a shows the schematic diagram of breakdown test and test results. The breakdown voltage test results show that the voltage resistance increases gradually with the increase of PVA content, which may be due to the more uniform and dense structure of PVA network and PAAm network, which is not easy to be breakdown. Secondly, the breakdown strength of DN-gel-3@nCW reached 238 kV/m after the addition of nCW, which was slightly higher than that of DN-gel-3. Higher withstand voltage can be used as a good reference for the selection of polarization voltage, which is beneficial to the polarization of dipoles and the capture and storage of deep-well charge in polymers.

Based on the mechanism of electrostatic induction, we designed devices as shown in Fig. 4b to characterize the charge density and charge retention rate of flexible bioelectrets. The electret, thickness H, is attached with a bottom electrode. The top electrode is not attached to the electret. As the top electrode moves down and up, we record the charge flowing between the two electrodes as a function of time, using a charge meter (Kistler 5018) and an oscilloscope (KEYSIGHT DSO1004A). According to the test results of breakdown voltage, the polarization field strength was set as 200 kV/m, and the effects of different temperatures on DN-gel-3 and DN-gel-3@nCW electret were studied. It can be seen from Fig. 4c, the surface charge density of DN-gel-3 and DN-gel-3@nCW increases with increasing polarization temperature, which could be due to having the same base material. However, too high temperature will destroy the structure of carnauba wax microspheres. As can be seen from the microscopic diagram in Fig. S5, the internal structure of the 70 °C and 80 °C composites changes significantly. In addition, according to DSC analysis of CW, softening and gradual phase transformation begin at about 60 °C (as shown in Fig. S3c), and the continuous increase of temperature in the process of polarization caused serious damage to the microsphere structure. Thus, the structure of nCW is destroyed when the

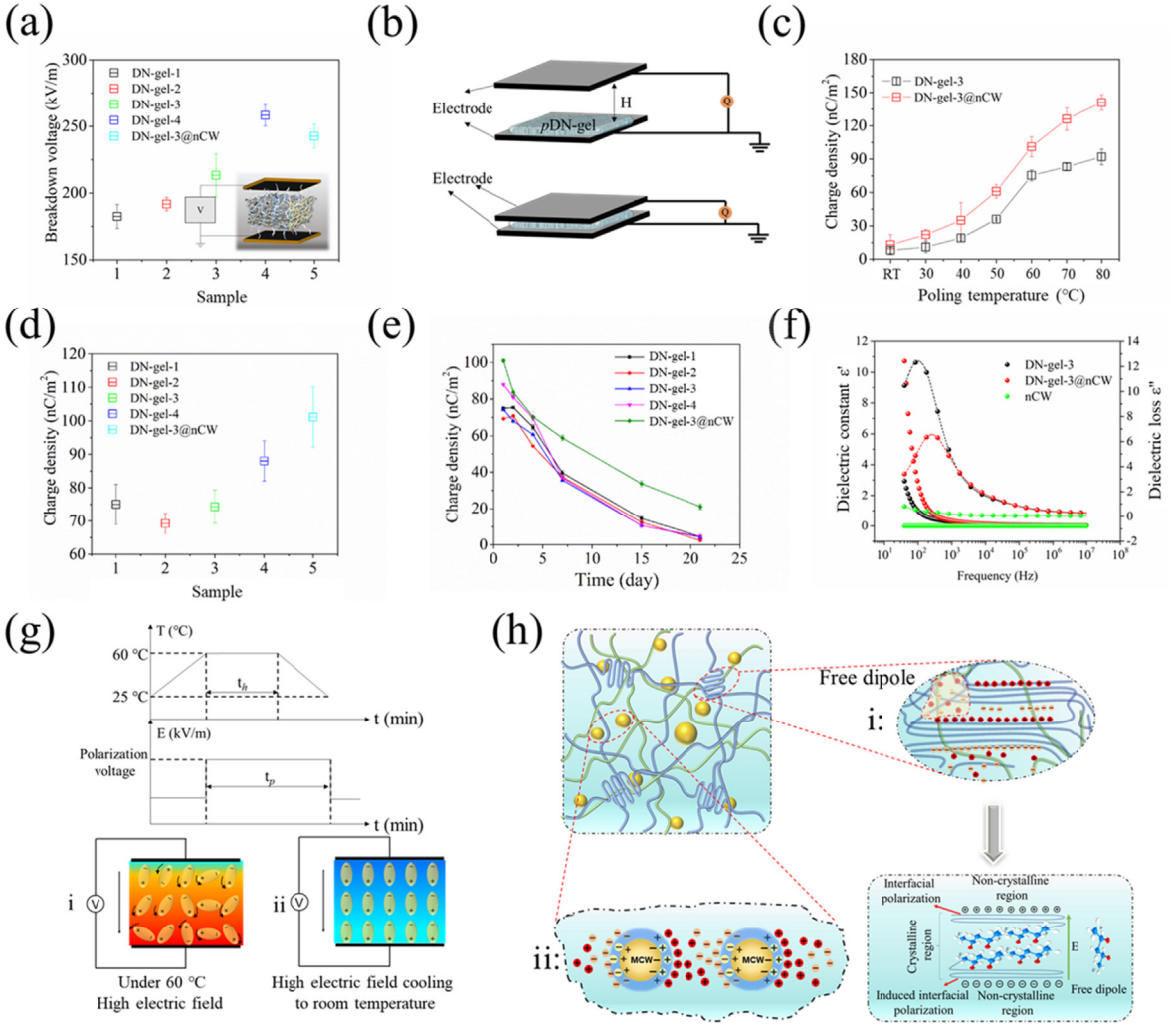

Fig. 4. Poling characteristics. (a) Diagram of breakdown test device for composite gels and breakdown voltage for different composite gels. (b) Schematic diagram of surface charge density measurement. When the upper plate is near or away from the film, the charge is captured and passed through a charge amplifier connected to the upper and lower electrodes. (c) Charge density of *p*DN-gel-3 and *p*DN-gel-3@nCW at different polarization temperatures under 200 kV/m. (d) Charge density of different *p*DN-gel composites after polarization, data is obtained after 24h test. (e) Charge attenuation of different *p*DN-gel composites. (f) Dielectric constant (solid lines) and dielectric loss (dashed lines) of nCW, DN-gel-3, and DN-gel-3@nCW as a function of frequency at room temperature. (g) Schematic diagram of a thermal polarization-oriented freezing dipole. (h) Polarization charge distribution and charge conduction mechanism in *p*DN-gel flexible bioelectret.

temperature is higher than 60 °C, so 60 °C is selected as the polarization temperature. Fig. 4g shows the thermal polarization conditions and the thermal polarization directional freezing dipole schematic diagram. As shown in Fig. 4d, charge density of different the polarized DN-gel (*p*DN-gel) composites after polarization (data is obtained after 24h test), and Fig. 4e show that charge attenuation of different *p*DN-gel composites. In the *p*DN-gel-1 sample, due to the low content of PVA, the internal pores of the composite material are large (see Fig. 2a of SEM image). There are many shallow traps in the *p*DN-gel-1 composite, and after polarization, more shallow trap charges are produced, which makes the surface charge. However, with the passage of time, the shallow trap charges will be released rapidly and it is not easy to keep it. However, with the increase of PVA content, the holes in the composites decrease, the shallow trap charges decrease and the deep trap charges increase. On the other hand, under the action of high-voltage electric field, the interface polarization will also occur in the crystalline region of PVA structure, which will also enhance the internal polarization. However, the long-term charge retention rate of compound DN-gel is not ideal. After a week, it decreased by less than 50%, and after three weeks, the charge density retention rate is only 3.2 nC/m^2 (see Fig. 4e). The dielectric properties of inorganic nano-filler and high insulating inorganic filler doped into the polymer matrix can be higher than those of pure polymer nanocomposites [4,45,46]. This method is effective and easy to operate, and it has great research value and application prospects for improving the polarization properties of materials. Therefore, in order to improve the electret performance of flexible DN-gel, carnauba wax emulsion nanospheres were added to the matrix as insulation filler to improve the electret performance of the matrix. It can be seen from Fig. 4e that the composite material after adding nCW surface charge density of the polarized DN-gel-3@nCW (*p*DN-gel-3@nCW) sample is further increased by 9% compared with that of the DN-gel-3 sample. This is due to the electret characteristics of carnauba wax itself [3], and after microsphere treatment, the properties of nanocomposites can be controlled by controlling the particle size in the composite network structure.

Thermally stimulating discharge (TSD) is an important method to study charge-trapping characteristics in dielectrics [47–49]. Similarly, using the principle of electrostatic induction, the cumulative discharge curve of depolarized charges from electret thermal stimulation was tested. Firstly, one side of the electret is coated with a graphite electrode, and then sealed in insulating silica gel. Then, it is fixed on a hot stage temperature controller (XPS-330, Shanghai JiaHang Instruments Co. LTD) at 0.5 °C/min. The electrode output signal is received by a charge amplifier, and the oscilloscope collects data (see Fig. S6a). As can be seen from Fig. S6a, with the increase of temperature, the induced positive charge accumulated on the surface of the electrode gradually increases. When the two electrets are near 60 °C, the induced positive charge increases to the maximum, and after 60 °C, the internal depolarization of the material begins to produce negative charge on the electrode surface. For the *p*DN-gel-3 sample, it can be seen that after 60 °C, the molecular chain motion of continuous endothermic polymer increases (Fig. S6b), which may aggravate the space charge trap and dipole charge relaxation in the polymer. For the *p*DN-gel-3@nCW sample, the DSC results show that the movement of polymer chain slows down at 60°C–85 °C due to the existence of nCW. As can also be seen from Fig. S5b, the space charge trap and dipole charge relaxation of the sample obviously slow down at this temperature. After nCW was completely melted at 85 °C, the loss of molecular chain motion hindered the motion, induced negative charge to increase linearly and accelerated the depolarization.

Dielectric spectra provide information on dielectric relaxation. There are α-, β- and γ-relaxation in the dielectric, corresponding to the low frequency, medium frequency and high frequency respectively [48]. Fig. 4f shows the dielectric constant and dielectric loss of nCW, DN-gel-3, and DN-gel-3 varying with frequency from 40 Hz to 10^7 Hz. It is clear that the dielectric constant of all samples slowly decreases as the frequency increases from 40 Hz to 10 MHz. In addition, although the dielectric constant of nCW is very low, the dielectric constant of DN-gel added with nCW increases from 3.1 to 10.7. For DN-gel-3@nCW samples, large dielectric constant values can be observed in the low frequency region. This is because nCW increases the movement of two-phase space charges under this electric field and is trapped at the interface between defects, forming many dipole moments. Space charge polarization dominates in the low frequency region, and this polarization mechanism can be explained by the Maxwell Wagner model of dielectric behavior. Dielectric peaks appear in the DN-gel-3 and DN-gel-3@nCW samples at low frequencies. Here, the dielectric loss at low frequencies is mainly caused by the migration of space charges generated by interface polarization. Due to the composite of nCW particles in the matrix of DN-gel-3@nCW, the interface polarization is weakened and the motion of charges is suppressed, thereby reducing its dielectric loss at low frequencies. These dielectric results indicate that the addition of nCW increases the stability of the space charge.

Fig. 4h shows composite materials *p*DN-gel-3@nCW schematic diagram of internal trapped charge distribution: i) there are crystals and amorphous regions in the composite gel. Under the action of the applied electric field, the opposite sign charges are generated at both ends of the interface of PVA microcrystal area. The traps at the interface will capture the deposited charges, which can be similar to the charge of impurity particles in the dipolar oriented polarization material in the electret material, and will move directionally along the direction of the electric field [50]. Secondly, under the action of the external electric field, the impurity particles (free dipoles) in the substance will migrate in a certain direction, generally moving in the direction of the electric field, so they will be captured by the captured charge in the substance, which is generally different signal charges. ii) Under the double action of electric field and temperature field, the impurity ions in the particle medium of carnauba wax produce macroscopic displacement, and the free charges in the matrix are captured by traps near the particles, forming a space charge of different symbols, thus accumulating charges around the particles. In particular, two adjacent carnauba wax particles can be compared to local miniature capacitors [51].

3.4. Output charge signal of pDN-gel-3@nCW measurement by mechanical and ultrasonic stimuli

Like any dipole electret, the electret can generate electromechanical conduction through piezoelectric contact and electrostatic non-contact. For dipole electret, the change of electrical signal can be caused by stretching or compressing. Such electret can control the surface charge change through external physical and mechanical stimuli. We use carbon conductive adhesive as a stretchable electrode, which is plated on the bottom of the electret and sealed in Ecoflex (0030) insulating silica gel. The *p*DN-gel-3@nCW) electret film, 3.0 cm × 1.0 cm × 0.5 mm in size, and the bottom electrode is connected with charge amplifier. Here, the charge distribution inside the electret is changed through deformation, resulting in induced charges on the electrode surface. The induced charge flow is captured by the charge amplifier and recorded, which is the change in surface charge of the electret. Fig. 5a and d are schematic diagrams of electret surface charge testing devices by stretching and compressing, respectively. As shown in Fig. 5b observe the change of induced charges at different stretching rates. The results show that the unpolarized DN-gel-3@nCW is almost no charge change during cyclic stretching. Fig. 5c shows that the *p*DN-gel-3@nCW is an obvious induced charges change process. With the increase of stretching speed, the cumulative induced charge flow and curve of electric charges are collected by a charge amplifier and recorded by an oscilloscope. The fitted cumulative charge change curve is shown in Fig. 5g, when the stretching speed is 1.5 mm/s, the maximum cumulative charge change reaches 14.92 nC, which can generate an output current of 0.187 nA (see Table 1). Similarly, we also carried out comparative tests under cyclic compression, as shown in Fig. 5d. The unpolarized DN-gel-3@nCW is almost charge change during the experiment, and only a charge changes of about 1 nC is generated during the friction between the electrode and

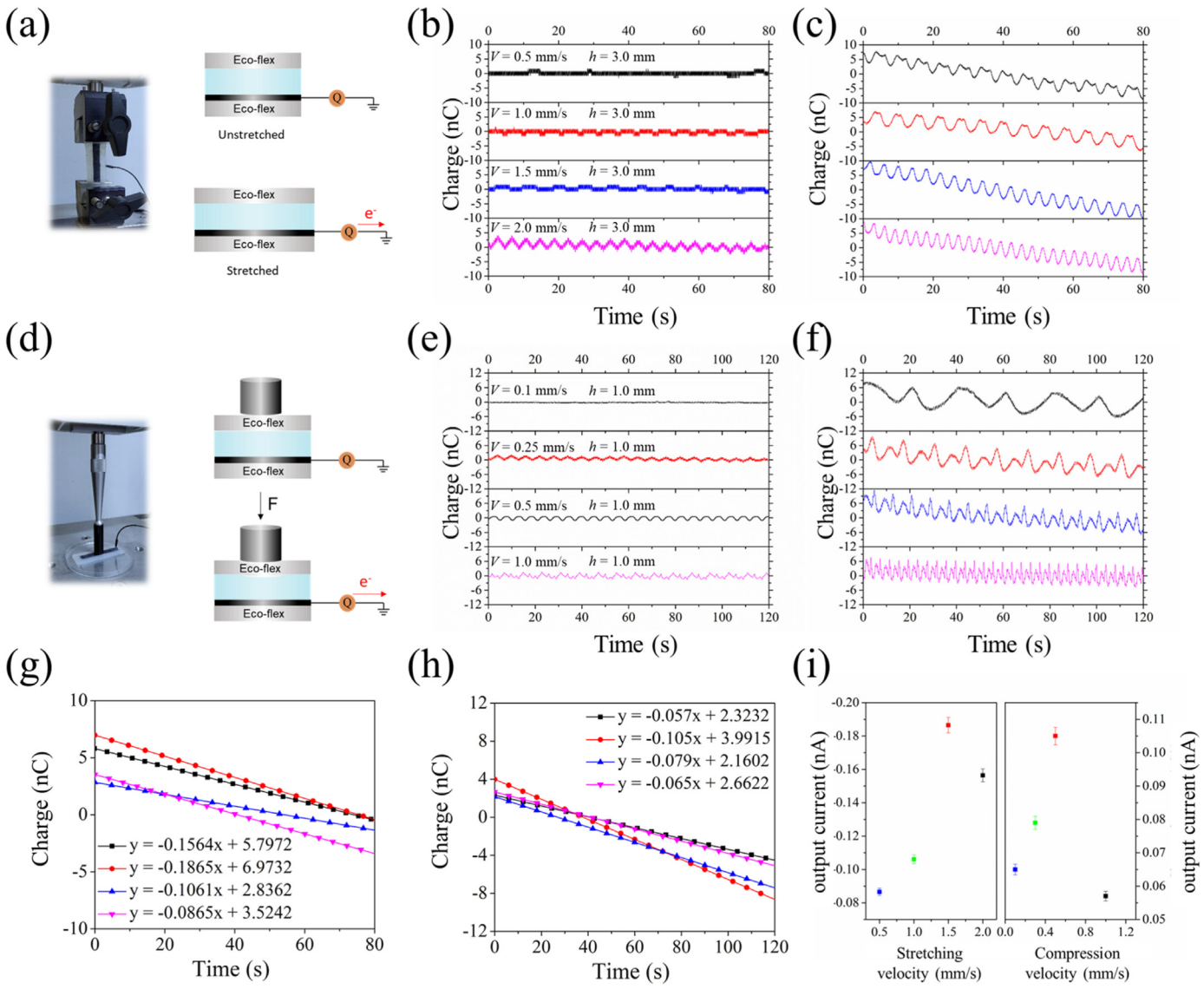

Fig. 5. External stimuli control mechanical and electrical conduction of the flexible bioelectret. Schematic diagram of electret surface charge test device (a) under stretch and (d) under compression. Electret surface charge of (b) unpolarized and (c) polarized DN-gel-3@nCW at different stretching frequencies. Electret surface charge of (e) unpolarized and (f) polarized DN-gel-3@nCW at different compression frequencies. Linear fit to charge change of *p*DN-gel-3@nCW under (g) stretching or (h) compression conditions. (i) Output current as a function of the frequency of stretching or compression.

Table 1
Electret charge change parameter of *p*DN-gel-3@nCW in electromechanical conduction under different cyclic stretching and cyclic compression.

Cyclic stretching rate (mm/s)	Cumulative charge flow[a] (nC)	Output current under cyclic stretching[a] (nA)	Cyclic compression rate (mm/s)	Cumulative charge flow[b] (nC)	Output current under cyclic compression[b] (nA)
0.5	6.92	0.087	0.1	7.80	0.065
1.0	8.49	0.106	0.25	9.48	0.079
1.5	14.92	0.187	0.5	12.60	0.105
2.0	12.51	0.156	1.0	6.84	0.057

[a] Linear fitting curve of change of electret surface charge from *p*DN-gel-3@nCW under cyclic stretching.
[b] Linear fitting curve of change of electret surface charge from *p*DN-gel-3@nCW under cyclic compression.

the material during the compression process for DN-gel-3@nCW. However, for *p*DN-gel-3@nCW, there is a similar rule as cyclic stretching, not that the faster the speed, the more charge is released. Through the linear fitting of *p*DN-gel-3@nCW cyclic compression charge change, in Fig. 5h, as can be seen that when the compression speed is 0.5 mm/s, the maximum accumulated charge flow amount reaches 12.60 nC, which can generate an output current of 0.105 nA. As can be seen from the above experimental results, the flexibility can be adjusted by stretching and compressing *p*DN-gel-3@nCW. During the process of under different cyclic stretching or cyclic compression, the change of the electret surface charge is relatively stable and continuously released.

In order to further explore the performance of physical stimulation on the surface charge of flexible electret, the electrical signal changes under different transmission powers of the oscillator (20 kHz, P_{max} = 1200 W)

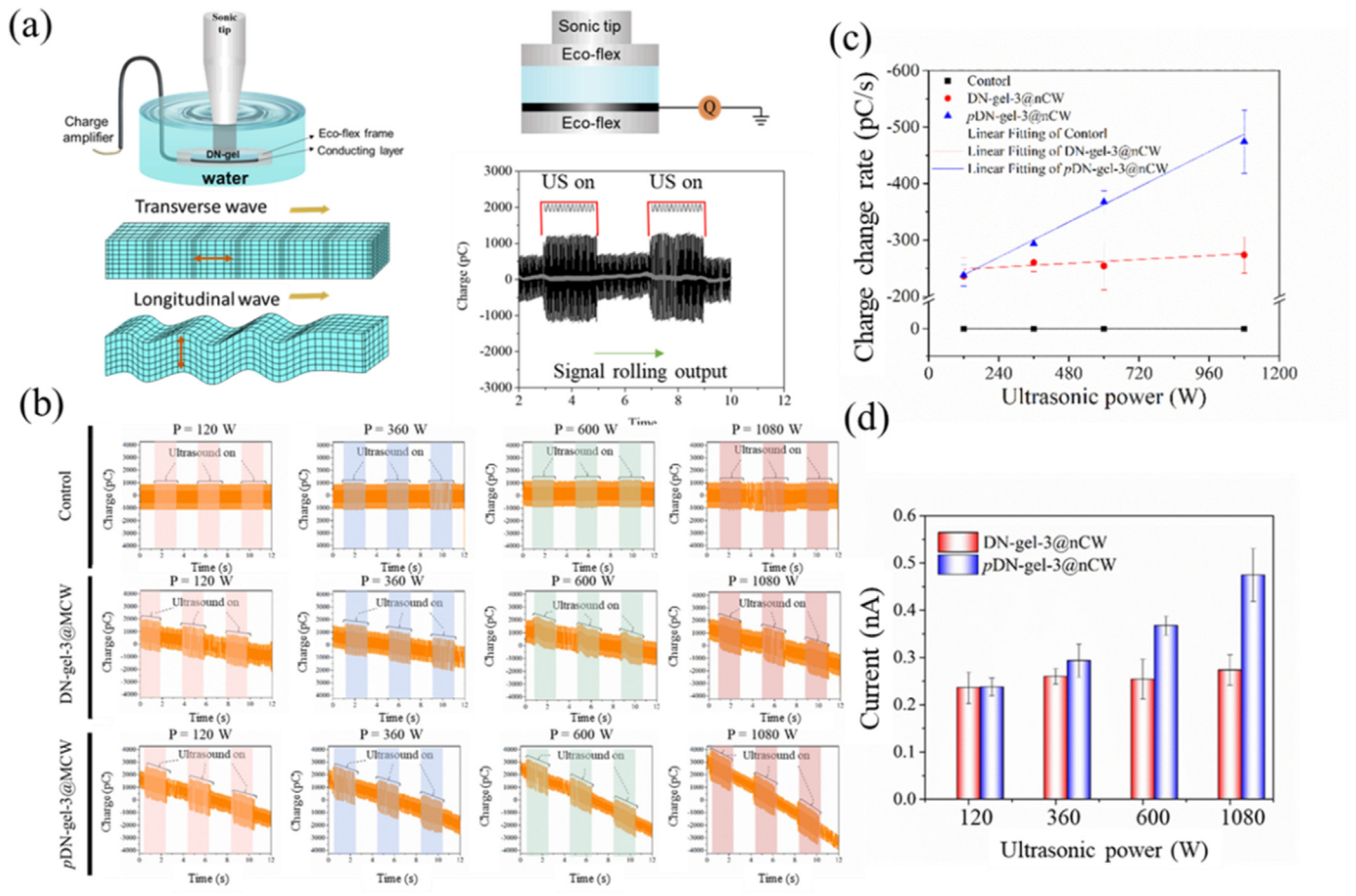

Fig. 6. Electric power generation by ultrasound propagation in *p*DN-gel-3@nCW. (a) Schematic diagram of ultrasonic stimulation electromechanical conduction device and the effect of ultrasonic on shear and longitudinal waves generated by *p*DN-gel-3@nCW. (b) Effect of different ultrasonic power on surface charge of unpolarized and polarized DN-gel-3@nCW. (c) The charge change rate and (d) output current as a function of ultrasonic power.

using ultrasonic as the stimulus source are shown in Fig. 6a. Fig. 6a shows the transverse wave and longitudinal wave generated by the emitted ultrasonic wave on the material. The transverse wave mainly generates tension similar to the horizontal direction on the material, while the longitudinal wave generates pressure in the vertical direction on the material. Fig. 6c shows the charge change rate curve of flexible electret under different ultrasonic emission power. The control group was under the action of ultrasound without electrodes. It can be seen that the ultrasonic stimulation did not produce changes in electrical signals, which ruled out the influence of friction electricity generation between materials and silica gel. For unpolarized DN-gel-3@nCW is charge change under the action of ultrasonic, but the charge change rate under different power is around −250 pC/s, which due to the electrical signal generated by the friction between the electrode and the material. Here, at 50% transmission power, the decrease in charge change rate may be caused by poor contact between the ultrasonic probe and the material. As shown in Fig. 6d, polarized DN-gel-3@nCW with the increase of ultrasonic power, the charge change rate increases gradually. When the ultrasonic power is 90%, the charge change rate reaches −472 pC/s, that is, the current of −0.472 nA is generated. It can be seen that flexible *p*DN-gel-3@nCW has ultrasonic electrical response, and change of electret surface charge can be controlled by adjusting ultrasonic emission power.

3.5. *Effects of ultrasonic stimulation of DN-gel-3@nCW bioelectret on drug release*

In the past thirty years, three kinds of electrically responsive drug delivery system (DDS) [52–54] have been developed: electrically responsive hydrogel, electrically conductive polymer and electrically responsive layer by layer (LBL) films. Hydrogel is made of polyelectrolyte, which usually expands or erodes under electric stimulation to release drugs. Conductive polymer can release charged drugs through partial oxidation or reduction. When stimulated and accompanied by drug release, LBL films was induced to dissolve or become unstable. Although great progress has been made in the field of electroactive drug delivery, there are still some shortcomings, which hinder its clinical transformation potential. Response hydrogel usually requires a relatively high voltage to trigger drug release, and long-term stimulation will cause adverse reactions (such as local inflammation). We innovatively put forward a gel material with long-term electret state as the drug carrier, which can stimulate drug release by ultrasonic wave on demand.

The material is polarized to keep it in a long-term electret state, and the drug release is regulated through ultrasonic stimulation, which also caused the change of local micro-electric field of the material. This feature will make it possible to develop drug delivery devices in the treatment of chronic diseases. Curcumin has a wide range of pharmacological activities. At present, curcumin reported in the literature has anti-inflammatory, anti-fibrosis, anti-oxidation, anti-depression, inhibition of renal vesicle formation, prevention and treatment of cancer and so on [55]. First, curcumin loaded nCW/Cur was obtained by lotion phase separation. As shown in Fig. S4, the characterization and analysis of FTIR, XRD, and DSC of nCW (no curcumin added), nCW/Cur, Cur, and physical mixture (carnauba wax and curcumin manually mixed) showed that curcumin was effectively encapsulated in a lipid matrix to obtain curcumin loaded particles. At the same time, the liposome loading rate can be regulated by controlling the ratio of curcumin to lipid matrix. As

shown in Table S2, with the increase of curcumin content, the loading rate gradually increases. Curcumin was loaded into carnauba wax nanospheres to construct a sustained-release drug system, and then *p*DN-gel-3@nCW/Cur was treated by thermal polarization. Here, the drug loading and stimulation parameters do not optimize the specific release amount at a specific time. On the contrary, we are concerned about the feasibility of regulating the release of curcumin from drug-loaded electrons by ultrasonic stimulation. In the above results, both physical and mechanical stimulation and ultrasonic stimulation have proved that the function of electret can regulate the release of electret electric signal. So, we use ultrasound to adjust the electrical signals and control drug release.

The in vitro release performance of Cur drug loaded membrane was evaluated in PBS buffer solution at 37 °C. As shown in Fig. 7a and b, curcumin is the drug release curve and Cur release rate curve at different time points without external stimulation. It can be seen that curcumin is released very quickly in the samples without carnauba wax nanospheres. The average release rate was 16%/h in the first 4 h, and the cumulative

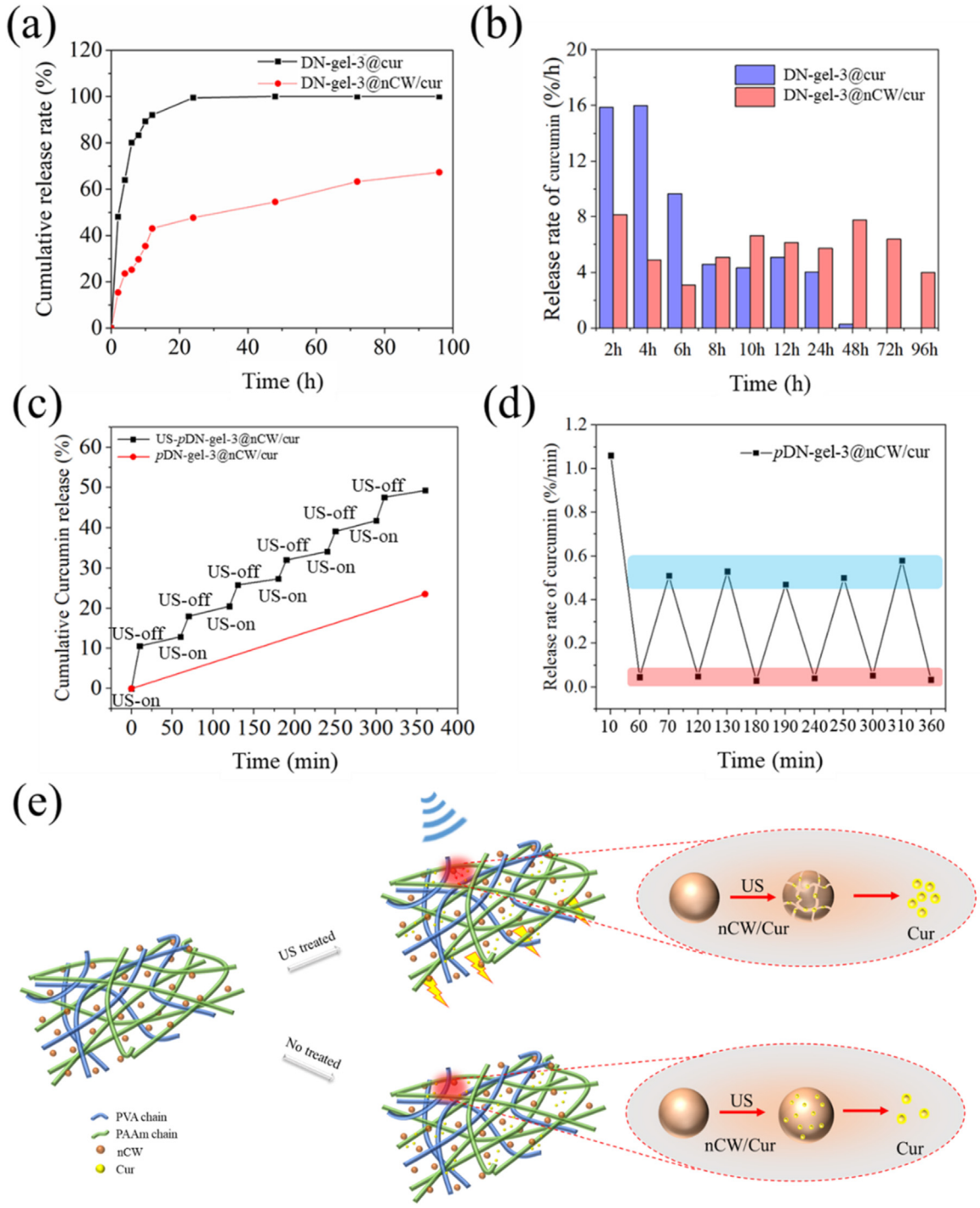

Fig. 7. Ultrasonic/electrical dual stimulation response for controlled drug release. (a) Cumulative release curve and (b) Cur release rate curve of drug-loaded membrane at different time points. (c) Cumulative release curve and (d) Cur release rate curve of drug-loaded membrane at different ultrasonic treatment time points. (e) Mechanism of accelerating Cur release from drug-loaded membranes by ultrasonic treatment.

release rate was 80% in the first 6 h. Curcumin was completely released within 24 h, which failed to achieve the desired effect in many practical applications. After being coated by carnauba wax nanospheres, the release rate of curcumin was higher in the first 2 h, which was due to the joint release of curcumin attached to the surface of the nanospheres and the shallow layer. After 6 h, the cumulative release rate was only 23%, and after 6 h, the release rate tended to be stable, with an average release rate of 6%/h, and no sudden release. The sustained release effect was good. In order to improve the utilization rate of drugs, the sustained release rate of organisms, such as the sustained release system of painkillers and local anesthetics [56,57], and the sustained release of drugs used for chronic inflammatory diseases (multiple sclerosis [58], arthritis [59] and wounds that are difficult to heal [60]) have been accepted. It can be seen that curcumin loaded on carnauba wax nanospheres can achieve long-term drug release, which not only reduces the side effects of drug burst, but also can achieve better therapeutic effect.

In order to study the release behavior of Cur carrier materials triggered by ultrasound, we used ultrasound as stimulation to treat Cur drug carrier membranes. Fig. 7c and d shows the cumulative release Curve of Cur after ultrasonic treatment and the release speed of cur at different ultrasonic time points. It can be seen that without ultrasonic treatment, the release amount of Cur is very low within 30 min, but after ultrasonic treatment for 10 min, the release amount of Cur suddenly increases. After ultrasonic treatment, the amount of release increased slowly. Therefore, composite drug-loaded membranes have the characteristics of ultrasonic response and is sensitive to ultrasonic signal. Ultrasonic treatment can effectively trigger the release of Cur from the matrix material. As can be seen from Fig. 8d that when the ultrasound is turned on, the release rate of Cur increases rapidly, and when the ultrasound is turned off, the release rate of Cur decreases significantly, indicating that the drug carrier film has ultrasonic response characteristics. Cur attached to the surface and shallow layer of drug-loaded nanospheres was released rapidly after the first ultrasonic treatment, and the release rate reached 1.06%/min. At the subsequent ultrasonic time point, the average release rate was 0.52%/min, and it had stable ultrasonic response release. Therefore, the release rate of Cur can be accurately controlled by controlling the time when the ultrasonic wave is turned on. Fig. 7e show mechanism of accelerating Cur release from drug-loaded membranes by ultrasonic treatment. Mechanical thermal effect caused by ultrasound and the accelerated degradation of matrix materials are the main reasons for accelerated release of Cur [61]. Moreover, in Fig. S7, a micro-electronic picture of the nCW particle state before and after ultrasonic treatment for

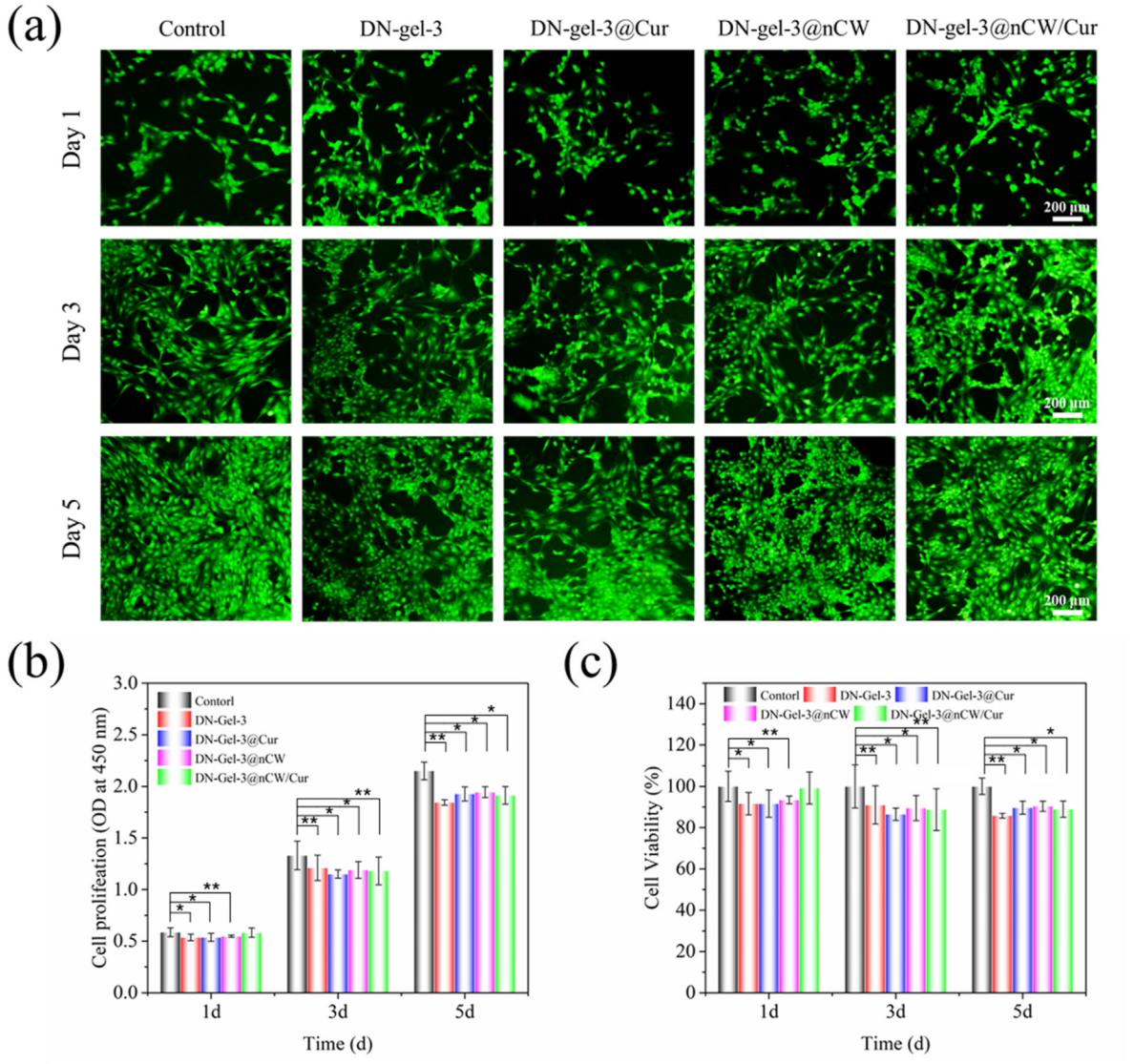

Fig. 8. Biocompatibility properties. (a) Calcein AM staining for live cells. Results of CCK-8 assay: OD values (b) and cell viability (c). $^{*}P < 0.05$ compared with blank control, $^{**}P < 0.01$ compared with blank control.

10min is reflected. It can be seen that under the action of ultrasound, some nCW particles are cracked. At the same time, the mechanical effects of ultrasound will produce electrical signals on flexible electronics (the above experiments have proved). Previous studies have shown that the electrical signals of electrons may cause the polarization of drug molecules, change the electrification of drug molecules, and thus change the fluidity and release rate [62]. Ultrasonic as a means to stimulate the drug-carrying film to release drugs, coupled with the electret material's unique electrical signal, here ultrasonic as an incentive of electret electrical signal release to produce a unique ultrasonic/electrical dual stimulation effect to achieve controllable and accurate release of drugs.

3.6. In vitro cytotoxicity of drug loading composites

Excellent biocompatibility and low cytotoxicity are also the important basis of biological applications of material. Calcein-AM staining and CCK-8 assay were conducted to evaluatethe potential cytotoxicity of DN-gel-3 composites on CCC-ESF-1. Fig. 8a exhibits live cells of different groups during the five days' incubation. On day 1, the number of living cells treated with DN-gel-3, DN-gel-3@Cur, DN-gel-3@nCW and DN-gel-3@nCW/Cur samples is almost the same as that of controls group. On day 3, the number of live cells treated with the extracts of DN-gel-3 and DN-gel-3@Cur decreased compared with other groups. The trends almost kept the same on day 5. DN-gel-3@Cur group showed the smallest cell number, DN-gel-3, DN-gel-3@nCW and DN-gel-3@nCW/Cur composites revealed lower cytotoxicity on CCC-ESF-1. Fig. 8b displays the OD value at 450 nm detected by CCK-8 assay, and Fig. 8c depicts cell viability calculated by normalizing OD to that of the control. Fig. 8b displays that all groups of cells showed linear growth during culture. On day 1, the treatment of DN-gel-3, DN-gel-3@Cur and DN-gel-3@nCW extracts decreased cell viability to 88%, 91% and 93%, respectively. Treatment with extracts of DN-gel-3@nCW/Cur did not significantly reduce cell viability compared with control. As treatment time prolonged, cell viability decreased for all the experimental groups, but the cell viability was not lower than 85%.

4. Conclusion

In summary, a flexible and biocompatible drug loaded composite electret was successfully prepared by thermal polarization method. The double network structure of polymer nano size can stably "lock" the dipole like (nCW). The nano effect of nCW increases the charge trap density, and the "lock" dipole structure of polymer matrix improves the charge stability. This design based on double network polymer matrix locking dipole particles opens a new idea for the construction of polymer based bioelectret. At the same time, the stable output of different electrical signals is realized by using different driving stimulation methods, which provides a basis for the regulation of electrical signals in its practical application. On this basis, the continuous and stable release of drugs was achieved through the electrical effect and ultrasonic synergistic stimulation generated by ultrasound, and the precise and controllable release was achieved. This shows that the ultrasound electric double stimulus responsive electret has great potential for application in on-demand precise drug delivery/release.

Credit author statement

Junfei Li: Methodology, Formal analysis, Investigation, Data curation, Writing – original draft, Visualization. Yajie Xie: Methodology, Investigation, Formal analysis, Validation, Visualization. Xiaoran Zou: Methodology, Investigation. Zhengze Li: Investigation, Validation. Wenbo Liu: Investigation, Validation. Guodong Liu: Visualization, Writing - review, and editing. Mengjiao Ma: Investigation, Validation. Yudong Zheng: Validation, Supervision, Project administration, Funding acquisition.

Declaration of competing interest

The authors declare that they have no known competing financial interests or personal relationships that could have appeared to influence the work reported in this paper.

Data availability

Data will be made available on request.

Acknowledgements

This work is financially supported by the National Natural Science Foundation of China (nos. 51973018 and 52273119), Beijing Science and Technology Project (Z191100002019017).

Appendix A. Supplementary data

Supplementary data to this article can be found online at https://doi.org/10.1016/j.mtbio.2023.100665.

References

[1] S. Gray, Philos. Trans. R. Soc. London, Ser. A (1732) 285.
[2] O. Heaviside, Electrical Paper, Chelsea, new york, 1892, p. 488.
[3] M. Eguchi, Variation of electrical conductivity of oils and waxes, Proc. Phys. Math. Soc. Japan 1 (1919) 320–326.
[4] A. Zaszczynska, A. Gradys, P. Sajkiewicz, Progress in the applications of smart piezoelectric materials for medical devices, Polymers 12 (2020) 2754.
[5] A. Zaszczynska, P. Sajkiewicz, A. Gradys, Piezoelectric scaffolds as smart materials for neural tissue engineering, Polymers 12 (2020) 161.
[6] K. Maity, S. Garain, K. Henkel, D. Schmeißer, D. Mandal, Self-Powered human-health monitoring through aligned PVDF nanofibers interfaced skin-interactive piezoelectric sensor, ACS Applied Polymer Materials 2 (2020) 862–878.
[7] H. Zhou, Y. Zhang, Y. Qiu, H. Wu, W. Qin, Y. Liao, Q. Yu, H. Cheng, Stretchable piezoelectric energy harvesters and self-powered sensors for wearable and implantable devices, Biosens. Bioelectron. 168 (2020), 112569.
[8] C. Zhang, W. Wang, X. Hao, Y. Peng, Y. Zheng, J. Liu, Y. Kang, F. Zhao, Z. Luo, J. Guo, B. Xu, L. Shao, G. Li, A novel approach to enhance bone regeneration by controlling the polarity of GaN/alGaN heterostructures, Adv. Funct. Mater. 31 (2020), 2007487.
[9] H. Li, Z. Guo, S. Kuang, H. Wang, Y. Wang, T. Wu, Z.L. Wang, G. Zhu, Nanocomposite electret with surface potential self-recovery from water dipping for environmentally stable energy harvesting, Nano Energy 64 (2019), 103913.
[10] A. Bandyopadhyay, A. Shivaram, I. Mitra, S. Bose, Electrically polarized TiO2 nanotubes on Ti implants to enhance early-stage osseointegration, Acta Biomater. 96 (2019) 686–693.
[11] X. Wen, D. Li, K. Tan, Q. Deng, S. Shen, Flexoelectret: an electret with a tunable flexoelectriclike response, Phys. Rev. Lett. 122 (2019), 148001.
[12] C. Liu, P.C. Hsu, H.W. Lee, M. Ye, G. Zheng, N. Liu, W. Li, Y. Cui, Transparent air filter for high-efficiency PM2.5 capture, Nat. Commun. 6 (2015) 6205.
[13] T. Chen, X. Gao, J.Y. Zhang, J.L. Xu, S.D. Wang, Ultrasensitive ZnO nanowire photodetectors with a polymer electret interlayer for minimizing dark current, Adv. Opt. Mater. 8 (2019), 1901289.
[14] P. Wei, X. Li, L. Wang, N. Liu, S. He, Y. Ren, Y. Zhu, Y. Yang, G. Lu, L. Bu, Vertical-resolved composition and aggregation gradient of conjugated-Polymer@Insulator-matrix for transistors and memory, Advanced Electronic Materials 6 (2020), 1901156.
[15] N. Wu, X. Cheng, Q. Zhong, J. Zhong, W. Li, B. Wang, B. Hu, J. Zhou, Cellular polypropylene piezoelectret for human body energy harvesting and health monitoring, Adv. Funct. Mater. 25 (2015) 4788–4794.
[16] D. Rodrigues, A.I. Barbosa, R. Rebelo, I.K. Kwon, R.L. Reis, V.M. Correlo, Skin-integrated wearable systems and implantable biosensors: a comprehensive review, Biosensors 10 (2020) 79.
[17] G.-J. Chen, M.-F. Lei, H.-M. Xiao, L. Wu, Unique charge storage characteristics of FEP/THV/FEP sandwich electret membrane polarized by thermally charging Technology, Chin. Phys. Lett. 31 (2014), 127702.
[18] M.M.A.C. Moreira, I.N. Soares, Y.A.O. Assagra, F.S.I. Sousa, T.M. Nordi, D.M. Dourado, R.H. Gounella, J.P. Carmo, R.A.C. Altafim, R.A.P. Altafim, Piezoelectrets: a brief introduction, IEEE Sensor. J. 21 (2021) 22317–22328.
[19] X. Wan, P. Chen, Z. Xu, X. Mo, H. Jin, W. Yang, S. Wang, J. Duan, B. Hu, Z. Luo, L. Huang, J. Zhou, Hybrid-piezoelectret based highly efficient ultrasonic energy harvester for implantable electronics, Adv. Funct. Mater. (2022), 2200589.
[20] Y. Wang, R. Shi, P. Gong, J. Li, J. Li, D. Ao, P. Wang, Y. Yang, Y. Man, Y. Qu, Bioelectric effect of a chitosan bioelectret membrane on bone regeneration in rabbit cranial defects, J. Bioact. Compat Polym. 27 (2012) 122–132.
[21] Y. Tu, X. Wang, Y. Lu, H. Zhang, Y. Yu, Y. Chen, J. Liu, Z. Sun, L. Cui, J. Gao, Y. Zhong, Promotion of the transdermal delivery of protein drugs by N-trimethyl

chitosan nanoparticles combined with polypropylene electret, Int. J. Nanomed. 11 (2016) 5549–5561.
[22] R. Okabayashi, M. Nakamura, T. Okabayashi, Y. Tanaka, A. Nagai, K. Yamashita, Efficacy of polarized hydroxyapatite and silk fibroin composite dressing gel on epidermal recovery from full-thickness skin wounds, J. Biomed. Mater. Res. B Appl. Biomater. 90 (2009) 641–646.
[23] X. Li, Y. Wang, M. Xu, Y. Shi, H. Wang, X. Yang, H. Ying, Q. Zhang, Polymer electrets and their applications, J. Appl. Polym. Sci. 138 (2020), 50406.
[24] W. Yanying, Q. Yili, G. Ping, W. Ping, M. Yi, L. Jidong, Preparation and in vitro evaluation of chitosan bioelectret membranes for guided bone regeneration, J. Bioact. Compat Polym. 25 (2010) 622–633.
[25] X. Shi, B. Deng, C. Sun, Single polar compound bio-electret and its influence on the cell growth, in: International Symposium on Electrets, 1997.
[26] S.B. Gong, B.W. Zhang, J.X. Zhang, Z.L. Wang, K.L. Ren, Biocompatible poly(lactic acid)-based hybrid piezoelectric and electret nanogenerator for electronic skin applications, Adv. Funct. Mater. 30 (2020), 1908724.
[27] N. Horiuchi, K. Madokoro, K. Nozaki, M. Nakamura, K. Katayama, A. Nagai, K. Yamashita, Electrical conductivity of polycrystalline hydroxyapatite and its application to electret formation, Solid State Ionics 315 (2018) 19–25.
[28] A. Ehterami, M. Kazemi, B. Nazari, P. Saraeian, M. Azami, Fabrication and characterization of highly porous barium titanate based scaffold coated by Gel/HA nanocomposite with high piezoelectric coefficient for bone tissue engineering applications, J. Mech. Behav. Biomed. Mater. 79 (2018) 195–202.
[29] S. Zhang, Y. Wang, X. Yao, P. Le Floch, X. Yang, J. Liu, Z. Suo, Stretchable electrets: nanoparticle-elastomer composites, Nano Lett. 20 (2020) 4580–4587.
[30] S.M. Peng, J.L. He, J. Hu, X.Y. Huang, P.K. Jiang, Influence of functionalized MgO nanoparticles on electrical properties of polyethylene nanocomposites, Ieee T Dielect El In 22 (2015) 1512–1519.
[31] S. Peng, B. Dang, Y. Zhou, J. Hu, J. He, Functionalized TiO2 nanoparticles tune the aggregation structure and trapping property of polyethylene nanocomposites, J. Phys. Chem. C 120 (2016) 24754–24761.
[32] X. Huang, P. Jiang, Y. Yin, Nanoparticle surface modification induced space charge suppression in linear low density polyethylene, Appl. Phys. Lett. 95 (2009), 242905.
[33] T. Mizutani, Behavior of charge carriers in organic insulating materials, in: Annual Report Conference on Electrical Insulation and Dielectric Phenomena, 2006, pp. 1–10, 2006.
[34] M.H. Al-Saleh, Carbon-based polymer nanocomposites as dielectric energy storage materials, Nanotechnology 30 (2019), 062001.
[35] M. Singh, I.E. Apata, S. Samant, W. Wu, B.V. Tawade, N. Pradhan, D. Raghavan, A. Karim, Nanoscale strategies to enhance the energy storage capacity of polymeric dielectric capacitors: review of recent advances, Polym. Rev. 62 (2021) 211–260.
[36] M.S. Kang, M. Kwon, H.J. Jang, S.J. Jeong, D.-W. Han, K.S. Kim, Biosafety of inorganic nanomaterials for theranostic applications, Emergent Materials 5 (2022) 1995–2029.
[37] E. Gonzalez-Mira, M.A. Egea, E.B. Souto, A.C. Calpena, M.L. Garcia, Optimizing flurbiprofen-loaded NLC by central composite factorial design for ocular delivery, Nanotechnology 22 (2011), 045101.
[38] J. Li, Z. Suo, J.J. Vlassak, Stiff, strong, and tough hydrogels with good chemical stability, J. Mater. Chem. B 2 (2014) 6708–6713.
[39] Y. Zhang, M. Song, Y. Diao, B. Li, L. Shi, R. Ran, Preparation and properties of polyacrylamide/polyvinyl alcohol physical double network hydrogel, RSC Adv. 6 (2016) 112468–112476.
[40] N. Yuan, L. Xu, H. Wang, Y. Fu, Z. Zhang, L. Liu, C. Wang, J. Zhao, J. Rong, Dual physically cross-linked double network hydrogels with high mechanical strength, fatigue resistance, notch-insensitivity, and self-healing properties, ACS Appl. Mater. Interfaces 8 (2016) 34034–34044.
[41] N. Pandey, S. Surana, S.K. Shukla, N.B. Singh, Methylene blue removal on nano-Fe3O4/poly(vinyl alcohol)/polyacrylamide hydrogel, Emerg. Mater. Res. 6 (2017) 305–313.
[42] M.C. Popescu, Structure and sorption properties of CNC reinforced PVA films, Int. J. Biol. Macromol. 101 (2017) 783–790.
[43] B.A.d. Rocha, C.R.L. Francisco, M.d. Almeida, F.Q. Ames, E. Bona, F.V. Leimann, O.H. Gonçalves, C.A. Bersani-Amado, Antiinflammatory activity of carnauba wax microparticles containing curcumin, J. Drug Deliv. Sci. Technol. 59 (2020), 101918.
[44] J.C. Viana, Polymeric materials for impact and energy dissipation, Plast., Rubber Compos. 35 (2013) 260–267.
[45] Y. Suzuki, D. Miki, M. Edamoto, M. Honzumi, A MEMS electret generator with electrostatic levitation for vibration-driven energy-harvesting applications, J. Micromech. Microeng. 20 (2010), 104002.
[46] X. Ma, X. Zhang, Vibration energy harvesting with stretchable electrets, in: IEEE International Conference on Dielectrics, 2018.
[47] G. Chen, J. Zhang, X. Shi, H. Peng, X. Chen, Charge trapped mechanism for semi-crystalline polymer electrets: quasi-dipole model, IET Nanodielectrics 3 (2020) 81–87.
[48] C. Li, G. Chen, X. Qiu, M. Gao, R. Gerhard, Modified polytetrafluoroethylene: towards easy-to-process space-charge electret materials, APEX 13 (2020).
[49] X. Huiming, C. Gangjin, C. Xumin, C. Zhi, A flexible electret membrane with persistent electrostatic effect and resistance to harsh environment for energy harvesting, Sci. Rep. 7 (2017) 8443.
[50] A.A. Gulyakova, Y.A. Gorokhovatsky, P. Frubing, R. Gerhard, Relaxation processes determining the electret stability of high-impact polystyrene/titanium-dioxide composite films, Ieee T Dielect El In 24 (2017) 2541–2548.
[51] N. Xu, Q. Zhang, H. Yang, Y. Xia, Y. Jiang, In-situ preparation of hierarchical flower-like TiO2/carbon nanostructures as fillers for polymer composites with enhanced dielectric properties, Sci. Rep. 7 (2017), 43970.
[52] M. Bansal, A. Dravid, Z. Aqrawe, J. Montgomery, Z. Wu, D. Svirskis, Conducting polymer hydrogels for electrically responsive drug delivery, J. Contr. Release 328 (2020) 192–209.
[53] M. Antensteiner, M. Khorrami, F. Fallahianbijan, A. Borhan, M.R. Abidian, Neural devices: conducting polymer microcups for organic bioelectronics and drug delivery applications, Adv. Mater. (2017) 29, 39/2017), Advanced Materials.
[54] X. Zhang, T. Liang, Q. Ma, Layer-by-Layer assembled nano-drug delivery systems for cancer treatment, Drug Deliv. 28 (2021) 655–669.
[55] L. Yixuan, M.A. Qaria, S. Sivasamy, S. Jianzhong, Z. Daochen, Curcumin production and bioavailability: a comprehensive review of curcumin extraction, synthesis, biotransformation and delivery systems, Ind. Crop. Prod. (2021) 172.
[56] H. Wang, Y. Zhang, X. Xu, A. Wang, An injectable mesoporous silica-based analgesic delivery system prolongs the duration of sciatic nerve block in mice with minimal toxicity, Acta Biomater. 135 (2021) 638–649.
[57] M. Pitorre, H. Gonde, C. Haury, M. Messous, J. Poilane, D. Boudaud, E. Kanber, G.A. Rossemond Ndombina, J.P. Benoit, G. Bastiat, Recent advances in nanocarrier-loaded gels: which drug delivery technologies against which diseases? J. Contr. Release 266 (2017) 140–155.
[58] C.T. Bever, S.I. Judge, Sustained-release fampridine for multiple sclerosis, Expet Opin. Invest. Drugs 18 (2009) 1013–1024.
[59] H. Huang, Z. Lou, S. Zheng, J. Wu, Q. Yao, R. Chen, L. Kou, D. Chen, Intra-articular drug delivery systems for osteoarthritis therapy: shifting from sustained release to enhancing penetration into cartilage, Drug Deliv. 29 (2022) 767–791.
[60] Z. Zeng, C. Guo, D. Lu, Z. Geng, D. Pei, S. Yu, Polyphenol–Metal Functionalized Hydrogel Dressing with Sustained Release, Antibacterial, and Antioxidant Properties for the Potential Treatment of Chronic Wounds, Macromolecular Materials and Engineering , n/a 2200262.
[61] T. Kang, F. Li, S. Baik, W. Shao, D. Ling, T. Hyeon, Surface design of magnetic nanoparticles for stimuli-responsive cancer imaging and therapy, Biomaterials 136 (2017) 98–114.
[62] B. Tandon, A. Magaz, R. Balint, J.J. Blaker, S.H. Cartmell, Electroactive biomaterials: vehicles for controlled delivery of therapeutic agents for drug delivery and tissue regeneration, Adv. Drug Deliv. Rev. 129 (2018) 148–168.